SCIENTIFIC REPORTS

OPEN

Conductivity-limiting bipolar thermal conductivity in semiconductors

Received: 28 October 2014
Accepted: 30 March 2015
Published: 13 May 2015

Shanyu Wang[1,*], Jiong Yang[1,*], Trevor Toll[1], Jihui Yang[1], Wenqing Zhang[2] & Xinfeng Tang[3]

Intriguing experimental results raised the question about the fundamental mechanisms governing the electron-hole coupling induced bipolar thermal conduction in semiconductors. Our combined theoretical analysis and experimental measurements show that in semiconductors bipolar thermal transport is in general a "conductivity-limiting" phenomenon, and it is thus controlled by the carrier mobility ratio and by the minority carrier partial electrical conductivity for the intrinsic and extrinsic cases, respectively. Our numerical method quantifies the role of electronic band structure and carrier scattering mechanisms. We have successfully demonstrated bipolar thermal conductivity reduction in doped semiconductors via electronic band structure modulation and/or preferential minority carrier scatterings. We expect this study to be beneficial to the current interests in optimizing thermoelectric properties of narrow gap semiconductors.

Thermal conduction in solids is one of the most fundamental physical processes. It reveals the nature of lattice dynamics as well as phonon scattering mechanisms. Thermal conductivity of solids also influences many technologically important topics including thermal insulation and management of energy storage and conversion systems, microelectronics, data storage devices; efficiency of thermoelectric materials; and stability of sensors and actuators. For semiconductors the low temperature thermal conductivity is not substantially distinct from those of insulators; at elevated temperatures, however, it becomes interesting and yet intriguing due to the vital roles of charge carriers and their interactions. A signature of electron-hole coupling in semiconductors is the bipolar thermal conduction at elevated temperatures, when the calculated lattice thermal conductivity (κ-$L\sigma$T, where κ is the total thermal conductivity, L the Lorenz number, σ the electrical conductivity, and T the absolute temperature) is significantly higher than the T^{-1} temperature dependence expected for phonon-phonon interaction dominated thermal conductivity[1–7]. Similar effect has also been found in semimetals[8–10]. For intrinsic semiconductors, it is well recognized that the mobility ratio between electrons and holes ($b = \mu_n/\mu_p$) determines the bipolar thermal conductivity (κ_b), which maximizes when $b = 1$[11,12]. Consequently, κ_b is insignificant for InSb, primarily due to its very large mobility ratio ($b > 100$)[13]. In the case of heavily doped semiconductors, the mobility ratio however is no longer a valid guide for understanding or predicting κ_b, due to the substantially different majority and minority carrier concentrations. For example, recent experiments showed significant κ_b in *p-type* heavily-doped skutterudites despite of the mobility ratio between two carriers being greater than 10 (hole mobility ~1–5 cm^2/V-s with a concentration of ~10^{21} cm^{-3} and electron mobility ~30–50 cm^2/V-s with a concentration of ~10^{18}–10^{19} cm^{-3} at 800 K, according to our numerical analyses which are presented below)[14–18], while the *n-type* skutterudites do not show appreciable κ_b, consistent with the rather small b value (~1/50)[19–29]. Similar observations have been reported for many

[1]Materials Science and Engineering Department, University of Washington, Seattle, WA 98195-2120, USA. [2]State Key Laboratory of High Performance Ceramics and Superfine Microstructure, Shanghai Institute of Ceramics, Chinese Academy of Sciences, Shanghai 200050, China. [3]State Key Laboratory of Advanced Technology for Materials Synthesis and Processing, Wuhan University of Technology, Wuhan 430070, China. *These authors contributed equally to this work. Correspondence and requests for materials should be addressed to J.Y. (email: jihuiy@uw.edu) or W.Z. (email: wqzhang@mail.sic.ac.cn) or X.T. (email: tangxf@whut.edu.cn)

other semiconductors[30–39]. These intriguing results necessitate comprehensive understanding of κ_b in semiconductors. A recent report attempted to model κ_b in doped $Bi_2(Te_{0.85}Se_{0.15})_3$ crystals but was unable to capture the specific roles of electronic band structure and carrier scattering mechanisms on κ_b[35].

In this study we report a combined experimental and computational effort that focused on unraveling the general behavior of κ_b in semiconductors. A numerical method for modeling the temperature dependence of κ_b for intrinsic as well as extrinsic (heavily doped) semiconductors encompassing a wide range of band gap and electronic band structure has been developed. We find that κ_b in semiconductors is in general "conductivity-limiting". In analogous to the bipolar ionic conduction and multiple-step diffusion processes, in which the overall kinetics are determined (limited) by the lower rate species or processes, the bipolar thermal conduction is limited by the charge carrier with lower partial electrical conductivity[40,41]. Therefore, it is determined by the minority carrier partial electrical conductivity and by the mobility ratio ("mobility-limiting") in extrinsic and intrinsic semiconductors, respectively. In order to validate these findings, we experimentally demonstrated κ_b reduction based on electronic band structure modulation and preferential minority carrier scattering. These results largely broaden our understanding of thermal conduction in semiconductors as well as offer insights for optimizing thermoelectric properties of narrow gap semiconductors.

Results and Discussion

Bipolar thermal conductivity in semiconductors can be expressed as[1–4]

$$\kappa_b = \frac{\sigma_n \sigma_p}{\sigma_n + \sigma_p}(\alpha_p - \alpha_n)^2 T, \tag{1}$$

where σ_i and α_i (subscript $i = n, p$) are the partial electrical conductivity and Seebeck coefficient for electrons and holes, respectively. For a single parabolic band, the Seebeck coefficient of each carrier can be written as[42]

$$\alpha_i = \pm \frac{k_B}{e}\left[\xi_i - \frac{(\lambda_i + 5/2)F_{\lambda_i+3/2}(\xi_i)}{(\lambda_i + 3/2)F_{\lambda_i+1/2}(\xi_i)}\right], \tag{2}$$

where k_B is the Boltzmann constant, e the free electron charge, ξ the reduce Fermi energy, λ the carrier scattering parameter, F_x the Fermi integral of the order of x. Therefore $\xi_n + \xi_p = -E_g/k_BT$, where E_g is the band gap[4]. For acoustic phonon scattering ($\lambda = -1/2$), the term $(\alpha_n - \alpha_p)^2$ can be written as $\left(\frac{k_B}{e}\right)^2\left[\frac{E_g}{k_bT} + \frac{2F_1(\xi_n)}{F_0(\xi_n)} + \frac{2F_1(\xi_p)}{F_0(\xi_p)}\right]^2$ which is associated with the total energy carried by electron-hole pairs (band gap energy and kinetic energies). The electrical conductivity of each carrier is

$$\sigma_i = ie\mu_i, \tag{3}$$

where $i = n, p$ designates the carrier concentrations of electron and hole, respectively.

"Conductivity-Limiting" Bipolar Thermal Conductivity. To elucidate the bipolar thermal conduction behavior in semiconductors, we may rearrange Eq. (1) into (assuming acoustic phonon scattering $\lambda = -1/2$, which is valid for most thermoelectric materials)

$$\frac{\left(\frac{k_B}{e}\right)^2\left[\frac{E_g}{k_BT} + \frac{2F_1(\xi_p)}{F_0(\xi_p)} + \frac{2F_1(\xi_n)}{F_0(\xi_n)}\right]^2 T}{\kappa_b} = \frac{1}{\sigma_n} + \frac{1}{\sigma_p}. \tag{4}$$

For a given material at a fixed T, the variation of $\left[\frac{E_g}{k_BT} + \frac{2F_1(\xi_p)}{F_0(\xi_p)} + \frac{2F_1(\xi_n)}{F_0(\xi_n)}\right]^2$ as a function of ξ_p or ξ_n is rather negligible, while the carrier concentrations and the partial electrical conductivity σ_i (right side of Eq. (4)) could change by several orders of magnitude because of the activation behavior of the charge carriers. Here $2F_1(\xi_p)/F_0(\xi_p)$ and $2F_1(\xi_n)/F_0(\xi_n)$ are the reduced kinetic energies of holes (ε_p/k_BT) and electrons (ε_n/k_BT), respectively, which only slightly change their numerical values when varying the Fermi level[43]. To verify these analyses, numerical data for p-type skutterudites ($R_xFe_3NiSb_{12}$) with $E_g = 0.2$ eV, $m_p^* = 5\ m_0$, $m_n^* = 2\ m_0$, at 800 K are plotted in fig. 1, where m_p^*, m_n^*, and m_0 are the effective mass of holes, effective mass of electrons, and free electron mass, respectively. The details of the calculations will be discussed below. As shown in fig. 1(a), with increasing ξ_p from –1 (weakly-degenerate) to 2 (degenerate), $2F_1(\xi_p)/F_0(\xi_p) + 2F_1(\xi_n)/F_0(\xi_n)$ only increases from 4.2 to 5.3, ~25% increases; whereas p increases by a factor of ~10 and the minority carrier partial conductivity σ_n decreases by a factor of ~20. These suggest that for semiconductors in general, Eq. (1) or (4) can be approximated as $1/\kappa_b(T) \propto 1/\sigma_p(T) + 1/\sigma_n(T)$, therefore κ_b in semiconductors is actually "conductivity-limiting",

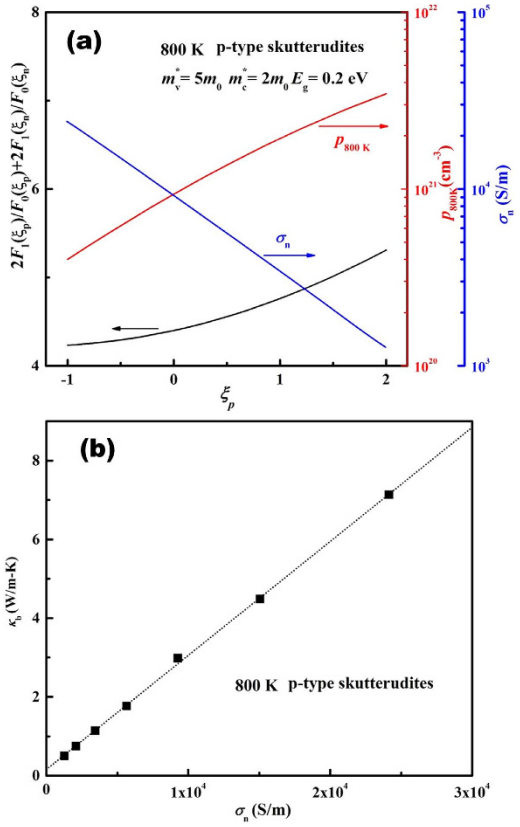

Figure 1. (**a**) Numerically calculated total reduced kinetic energy $2F_1(\xi_p)/F_0(\xi_p) + 2F_1(\xi_n)/F_0(\xi_n)$ for holes and electrons, hole (majority carrier) concentration, and electron (minority carrier) partial electrical conductivity as a function of the reduced Fermi level (ξ_p); (**b**) calculated κ_b as a function of minority carrier partial electrical conductivity σ_n. The dashed line is a guide for eye. The calculations were carried out for *p-type* skutterudites ($R_xFe_3NiSb_{12}$) with $E_g = 0.2$ eV, $m_p^* = 5m_0$, $m_n^* = 2m_0$, at 800 K.

analogous to the rate-limiting phenomena in kinetic diffusion processes[41]. For intrinsic semiconductors, since $n = p$, Eq. (4) can be further approximated to be $1/\kappa_b(T) \propto 1/\mu_p(T) + 1/\mu_n(T)$, consistent with the large body of literature already developed. In the case of extrinsic semiconductors ($n \gg p$ or $p \gg n$) κ_b is primarily determined by the partial electrical conductivity of the minority carriers, not by the mobility ratio. A linear dependence of κ_b vs. σ_n at 800 K for *p*-type doped skutterudites, as shown in fig. 1(b), further substantiates our proposed "conductivity-limiting" concept for bipolar thermal conduction in semiconductors.

Numerical Modeling. Data presented in fig. 1 were calculated by our numerical method for modeling the temperature dependence of κ_b in semiconductors. Our numerical method aimed at discerning the underlying physics that controls κ_b, including the electronic band structure features and carrier scattering mechanisms. We use the experimental carrier concentration values as those of the majority carriers. Based on the majority carrier concentration and Seebeck coefficient at room temperature, and the maximum Seebeck coefficient value at elevated temperatures, we can determine the Fermi level, the majority carrier effective mass and E_g[44,45]. The minority carrier effective mass is used as an adjustable parameter. The majority and minority carrier concentrations and their temperature dependences are calculated based on semiconductor statistics[46]. In order to obtain the T dependence of mobility, we first modeled its carrier concentration dependence at room temperature. We then assumed that the carriers are predominantly scattered by the acoustic phonons, therefore $\mu_i(T) = \mu_i(300\text{ K})(T/300\text{ K})^{-3/2}$ and $\lambda_n = \lambda_p = -1/2$. For example, the room temperature carrier mobility of *n-type* and *p*-type 3*d* transition metal-based skutterudite antimonides $R_x(Fe,Co,Ni)_4Sb_{12}$ as a function of carrier concentration is shown in fig. 2, where R represents fillers and x the filling fraction. The data were taken from the literatures[14–27,47–59] and were well represented by an empirical expression (the solid lines in fig. 2)[60]

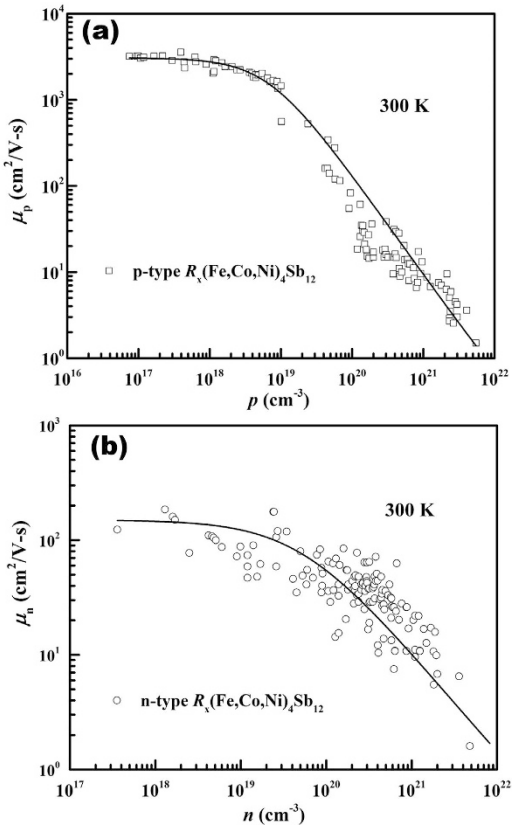

Figure 2. Room temperature carrier mobility as a function of carrier concentration for (**a**) *p-type* and (**b**) *n-type* $R_x(Fe,Co,Ni)_4Sb_{12}$ skutterudites. The solid lines are least squares fits to the data using Eq. (5). Data used here are taken from Refs. 14–27 and 47–59.

$$\mu_i(300\mathrm{K}) = \mu_i^{\,0} + \frac{\mu_i^{\,\max} - \mu_i^{\,0}}{1 + \left(\frac{i}{i_{\mathrm{Ref}}}\right)^a}, \tag{5}$$

where i_{Ref} is the reference carrier concentration, approximately where degeneracy sets in, a is a fitting parameter, and $\mu_i^{\,0}$ and $\mu_i^{\,\max}$ are the minimum and maximum possible mobility, respectively. In general, the carrier concentration dependence of mobility for all semiconductors studied in this work can be well accounted by this phenomenological formula and the fitting parameters are summarized in the Table S1 (Supporting Information, SI).

Based on Eqs. (1)–(3) and (5) and the aforementioned method, we were able to numerically fit the temperature dependence of κ_b in intrinsic and extrinsic semiconductors with a large variation of band gap, the Fermi level, and effective mass values. Figure 3(a) shows the excellent agreement between the experimental data (symbols) for intrinsic Si single crystal[7] and degenerate polycrystalline skutterudite $Yb_{0.7}Fe_3NiSb_{12}$ in a wide temperature range. Figure 3(b) shows the calculated (κ_b^{Cal}) and experimental (κ_b^{Exp}) values of κ_b for a variety of materials at various temperatures, including $(Bi,Sb)_2(Te,Se)_3$[37,61], skutterudites, Si, and Ge[6,7]. The dashed line in fig. 3(b) represents $\kappa_b^{Cal} = \kappa_b^{Exp}$. These results suggest that our method well accounts for the temperature dependence of κ_b in semiconductors (all relevant parameters used in our calculations are summarized in Table S2, SI). Since κ_b is determined by the minority carrier partial electrical conductivity in doped semiconductors, the minority carrier effective mass and its mobility, as well as E_g will have strong influence. The extent to which these parameters affect κ_b is illustrated in Fig. S1 (SI). This also suggests that κ_b modification can be achieved by manipulating these parameters.

Bipolar Thermal Conductivity Reduction. In order to examine the validity of the minority carrier dominated bipolar thermal conduction in heavily doped semiconductors, and to utilize the concept of modifying κ_b presented, we investigated ways of κ_b reduction motivated by the recent quest for high efficiency thermoelectric materials that necessitate low thermal conductivity[62–65]. It is well known that in filled skutterudites[66], the triple degenerate conduction band minimum (CBM) is primarily composed of

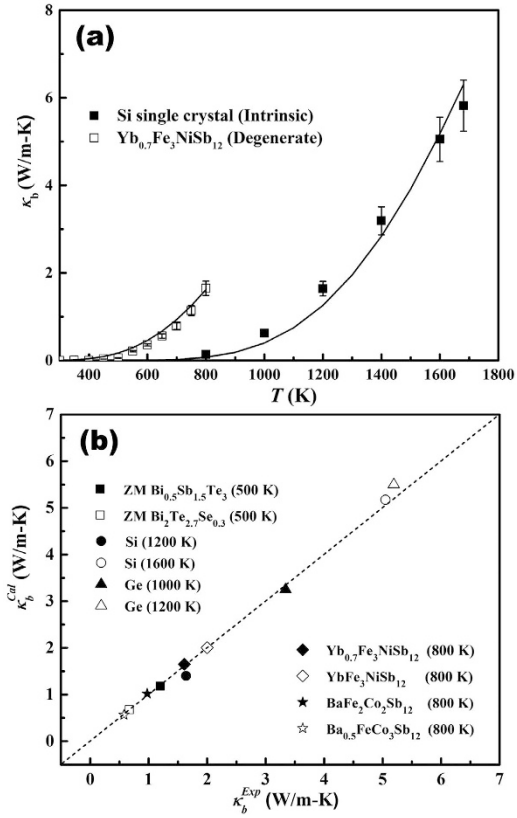

Figure 3. (**a**) Experimental (symbols) and fitted (solid lines) bipolar thermal conductivity of intrinsic Si single crystal and degenerate $Yb_{0.7}Fe_3NiSb_{12}$ vs. *T*. (**b**) Experimental (κ_b^{Exp}) and calculated (κ_b^{Cal}) bipolar thermal conductivity for intrinsic Si and Ge single crystals, and degenerate Bi_2Te_3-based zone melted (ZM) compounds and *p-type* skutterudites at various temperatures. The dashed line represents $\kappa_b^{Cal} = \kappa_b^{Exp}$.

d-orbitals from the transition metals (TMs), with some contribution from Sb *p*-states (*p-d* hybridization). Thus the density of states (DOS) at the CBM can be effectively adjusted by varying the TMs. Our first principles calculations reveal that in the *p*-type Ba-filled skutterudites, DOS at the CBM decreases significantly with decreasing Fe/Co ratio on the TM sites from 2:2 to 1:3, as shown in fig. 4(a), mainly due to the higher energy and thus more contribution of 3*d* orbitals of Fe as compared with those of Co. The distinct DOS of minority carrier band further suggests that κ_b for *p*-type $Ba_{0.5}Co_3FeSb_{12}$ should be smaller than $BaCo_2Fe_2Sb_{12}$ due to the minority carrier partial conductivity reduction. Data for 800 K κ_b vs. the majority carrier (hole) concentration for a series of $Ba_xCo_3FeSb_{12}$ and $Ba_yCo_2Fe_2Sb_{12}$ samples are plotted in fig. 4(b), and the lines represent fitting to the data using the minority carrier effective masses $m_n^* = 1.3m_0$ and $m_n^* = 2.2m_0$, respectively. This electronic band modulation induced κ_b reduction substantiates the dominant role of the minority carriers. Because of the commonly triple-degenerate and 3*d*-orbital-dominated nature of the CBM, the minority carrier effective masses of the *p-type* skutterudites are usually much higher than those of the *n-type*, in which the minority carrier band is mainly composed of single-degenerate Sb *p*-orbital-featured light bands[67]. Therefore, the predominant underlying reason for large differences in κ_b between the *n*- and *p*-type skutterudites is actually due to the effective mass differences between the corresponding conduction and valence (minority) bands.

Our second example of κ_b reduction takes the advantage of preferential scattering of the minority carriers. Normally in heavily doped semiconductors, the minority carriers are non-degenerate. Given the electronic band structure of a material and the Fermi level (determined by the majority carrier concentration), one can calculate the range of minority carrier wavelength[46]. For example, the electron wavelength in a heavily-doped *p-type* Bi_2Te_3 ($p = 3.5 \times 10^{19}\,cm^{-3}$) is approximately between 10 nm and 50 nm, as shown in fig. 5(a). We compare κ_b of *p*-type zone melted (ZM) and nanostructured (Nano) $Bi_{0.5}Sb_{1.5}Te_3$ prepared by the melt spinning combined with subsequent spark plasma sintering (MS-SPS) technique[61]. Figure 5(b) shows, at comparable majority carrier concentrations between the ZM and Nano samples, a significant κ_b reduction is achieved when nanoprecipitates are introduced into the sample. The minority carrier partial electrical conductivity is determined by E_g, minority effective mass and mobility. The estimated small E_g variation between ZM and Nano is only responsible for 20% of the κ_b reduction. For a large system like nanostructured $Bi_{0.5}Sb_{1.5}Te_3$, a full electronic band structure calculation

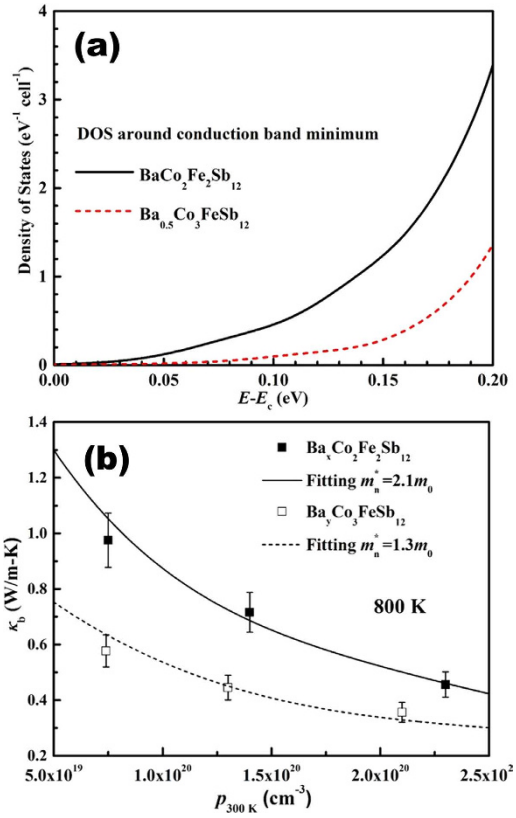

Figure 4. (**a**) The density of states around the CBM for $BaCo_2Fe_2Sb_{12}$ and $BaCo_3FeSb_{12}$. (**b**) Bipolar thermal conductivity at 800 K as a function of hole (majority carrier) concentration for $Ba_xCo_2Fe_2Sb_{12}$ and $Ba_yCo_3FeSb_{12}$. The lines in (**b**) are fits to the data using different minority carrier effective mass values.

is computationally unfeasible. It is difficult to directly determine m_n^* (minority carrier) at the CBM. The estimated m_n^* values of *n-type* doped ZM and Nano $Bi_2Te_{2.7}Se_{0.3}$ are 1.0 m_0 and 1.1 m_0, respectively[38,68]. If we assume comparable m_n^* at CBM between the ZM and Nano samples, the major part of κ_b reduction between the *p-type* ZM and Nano $Bi_{0.5}Sb_{1.5}Te_3$ with comparable majority hole concentrations could be attributed to the reduction of minority carrier mobility (μ_n) corroborated by our κ_b fittings, where $\mu_n = 4095\,cm^2/V\text{-}s$ for the ZM and $1115\,cm^2/V\text{-}s$ for the Nano. The TEM image (inset of fig. 5(b)) shows that the sizes of nanoprecipitates closely match those of the minority electron wavelengths. Given the majority hole wavelength is estimated to be ~2 nm, we postulate a strong preferential minority carrier scattering by the nanoprecipitates in the Nano $Bi_{0.5}Sb_{1.5}Te_3$. Similar κ_b reduction can also be observed in nanostructured *n-type* $Bi_2(Te,Se)_3$ compounds[38,69,70]. Extensive recent studies have established the role of nanostructure on lattice thermal conductivity reduction[63,65], we propose an "preferential minority carrier scatterings" for κ_b reduction, which is partially responsible for the thermoelectric performance gains reported, especially at elevated temperatures[61,71]. Recent theoretical work has also demonstrated that similar κ_b reduction via heterostructure barriers scattering is possible[72]. Finally we caution that nanostructure induced band structure modulation reported in $AgPb_mSbTe_{2-m}$ might be possible for $Bi_{0.5}Sb_{1.5}Te_3$[73], which could be responsible for part of the κ_b reduction.

Summary

To conclude, our combined theoretical analysis and experimental measurements have established that in semiconductors bipolar thermal transport is in general a "conductivity-limiting" phenomenon, which is controlled by the carrier mobility ratio and the minority carrier partial electrical conductivity for the intrinsic and extrinsic cases, respectively. The numerical method we developed quantifies the role of electronic band structure and carrier scattering mechanisms. We have also demonstrated feasible strategies for manipulating the bipolar thermal conductivity in doped semiconductors via electronic band structure modulation and/or preferential minority carrier scatterings. We expect our study to be beneficial to the current interests in optimizing thermoelectric properties of narrow gap semiconductors.

Methods

Samples in this study were synthesized by a combination of induction melting and long-term high-temperature annealing, by zone melting, or by MS-SPS, and the details of which were documented

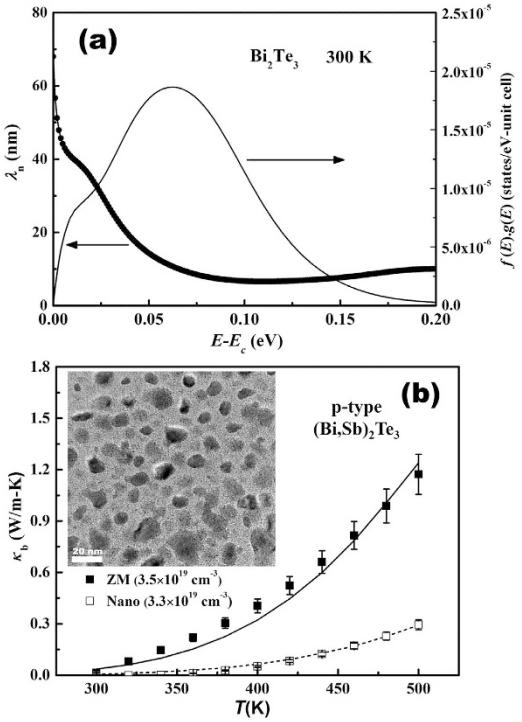

Figure 5. (**a**) The calculated electron wavelength, and the product of the Fermi-Dirac distribution function and electronic density of states *f(E) g(E)* vs. energy with the zero point corresponding to the conduction band minimum (E_c). (**b**) The experimental and modeled bipolar thermal conductivity vs. temperature, for *p-type* zone melted (ZM) and nanostructured (MS-SPS) $Bi_{0.5}Sb_{1.5}Te_3$. The inset is a TEM picture of the MS-SPS bulk sample which shows 10–50 nm nanoprecipitates. (The room temperature minority carrier mobilities of ZM and Nano samples are $\mu_n = 4095$ and 1115 cm^2/V-s, respectively).

elsewhere[19,61]. High-resolution transmission electron microscopy (TEM) images were collected using a JEM-2100F TEM. Electrical conductivity (σ) and Seebeck coefficient (α) were simultaneously measured by an Ulvac ZEM-3 under a low-pressure helium atmosphere. Thermal conductivity was calculated from the measured thermal diffusivity (D), specific heat (C_p), and density (d) using the relationship $\kappa = DC_pd$. Thermal diffusivity D was tested by laser flash diffusivity method using a Netzsch LFA-457 system, and C_p was measured by a Netzsch DSC 404F1 using sapphire as the reference. The accuracy of the κ measurements is estimated to be ~10% and the precision <5%. κ_b were extrapolated from $\kappa_b + \kappa_L = \kappa\text{-}L\sigma T$ by assuming lattice thermal conductivity κ_L is inversely proportional to T. Hall measurements were performed on a Janis cryostat equipped with a 9 Tesla superconducting magnet. The carrier concentration of electron (n) or hole (p) and the corresponding Hall mobility μ_n or μ_p (subscript n represents the electron and p the hole) were estimated from the measured Hall coefficient (R_H) and electrical conductivity by the relation $n, p = 1/e|R_H|$ and $\mu_{n,p} = \sigma|R_H|$, respectively.

The first-principles electronic band structure calculations were performed with the generalized gradient approximation functional of Perdew, Burke, and Ernzerhof[74], with projected augmented wave method[75,76], as implemented in Vienna *ab initio* simulation package (VASP)[77]. The computational techniques are similar to those published previously[66,78]. The de Broglie wavelengths (λ) is defined as, $\lambda = h/m^*v$, where h, m^*, and v are the Planck constant, carrier effective mass, and drift velocity, respectively. m^*, v and λ of degenerate majority carriers are almost energy independent (k_BT within the Fermi level), while for non-degenerate minority carriers these values are energy dependent, which are derived from band structure. The detailed calculation method is shown in Supporting Information, and the calculated density of state, m_n^* and v_n of electrons for *p-type* Bi_2Te_3 ($\xi_p = 0.25$, $m_p^* = 1.3\ m_0$) are shown in figure S2 (SI).

References

1. Price, P. Ambipolar thermodiffusion of electrons and holes in semiconductors. *Philos. Mag.* **46,** 1252–1260 (1955).
2. Davydov, B. & Shmushkewitch, J. Electrical conductivity of semi-conductors with an ionic lattice in strong fields. *J. Phys.* **3,** 359 (1940).
3. Goldsmid, H. The thermal conductivity of bismuth telluride. *Proceed. Phys. Soc. Sec. B* **69,** 203 (1956).
4. Drabble, J. R. & Goldsmid, H. J. *Thermal Conduction in Semiconductors*. (Pergamon Press, Oxford, 1961).
5. Berman, R. *Thermal Conduction in Solids*. (Clarendon Press, Oxford, 1976).
6. Slack, G. A. & Glassbrenner, C. Thermal conductivity of germanium from 3 °K to 1020 °K. *Phys. Rev.* **120,** 782 (1960).

7. Glassbrenner, C. & Slack, G. A. Thermal conductivity of silicon and germanium from 3 K to the melting point. *Phys. Rev.* **134,** A1058 (1964).
8. Gallo, C., Miller, R., Sutter, P. & Ure Jr, R. Bipolar Electronic Thermal Conductivity in Semimetals. *J. Appl. Phys.* **33,** 3144–3145 (1962).
9. Uher, C. & Goldsmid, H. Separation of the electronic and lattice thermal conductivities in bismuth crystals. *phys. stat. solid. (b)* **65,** 765–772 (1974).
10. Magomedov, A.-M. & Pashaev, B. Thermal conductivity of alloys of the bismuth-antimony system in solid and liquid states. *Sov. Phys. J.* **15,** 287–290 (1972).
11. Abeles, B. Thermal conductivity of germanium in the temperature range 300–1080 K. *J. Phys. Chem. Solids* **8,** 340–343 (1959).
12. Kettel, F. Die Wärmeleitfähigkeit von Germanium bei hohen temperaturen. *J. Phys. Chem. Solids* **10,** 52–58 (1959).
13. Bowers, R., Ure Jr, R., Bauerle, J. & Cornish, A. InAs and InSb as thermoelectric materials. *J. Appl. Phys.* **30,** 930–934 (1959).
14. Liu, R. *et al. p-Type* skutterudites $R_xM_yFe_3CoSb_{12}$ (R, M = Ba, Ce, Nd, and Yb): Effectiveness of double-filling for the lattice thermal conductivity reduction. *Intermetallics* **19,** 1747–1751 (2011).
15. Cho, J. Y. *et al.* Thermoelectric properties of p-type skutterudites $Yb_xFe_{3.5}Ni_{0.5}Sb_{12}$ ($0.8 < x < 1$). Acta *Mater.* **60,** 2104–2110 (2012).
16. Rogl, G. *et al.* Thermoelectric properties of p-type didymium (DD) based skutterudites $DD_y(Fe_{1-x}Ni_x)_4Sb_{12}$ ($0.13 < x < 0.25$, $0.46 < y < 0.68$). J. Alloy. *Compd.* **537,** 242–249 (2012).
17. Liu, R., Qiu, P., Chen, X., Huang, X. & Chen, L. Composition optimization of *p-type* skutterudites $Ce_yFe_xCo_{4-x}Sb_{12}$ and $Yb_yFe_xCo_{4-x}Sb_{12}$. *J. Mater. Res.* **26,** 1813–1819 (2011).
18. Qiu, P. *et al.* Effects of Sn-doping on the electrical and thermal transport properties of *p-type* Cerium filled skutterudites. *J. Alloy. Compd.* **509,** 1101–1105 (2011).
19. Shi, X. *et al.* Multiple-filled skutterudites: high thermoelectric figure of merit through separately optimizing electrical and thermal transports. *J. Am. Chem. Soc.* **133,** 7837–7846 (2011).
20. Ballikaya, S., Uzar, N., Yildirim, S., Salvador, J. R. & Uher, C. High thermoelectric performance of In, Yb, Ce multiple filled $CoSb_3$ based skutterudite compounds. *J. Solid State Chem.* **193,** 31–35 (2012).
21. Xiong, Z., Chen, X., Huang, X., Bai, S. & Chen, L. High thermoelectric performance of $Yb_{0.26}Co_4Sb_{12}$/yGaSb nanocomposites originating from scattering electrons of low energy. *Acta. Mater.* **58,** 3995–4002 (2010).
22. Bai, S. *et al.* Enhanced thermoelectric performance of dual-element-filled skutterudites $Ba_xCe_yCo_4Sb_{12}$. *Acta. Mater.* **57,** 3135–3139 (2009).
23. Zhao, X. *et al.* Synthesis and thermoelectric properties of Sr-filled skutterudite $Sr_yCo_4Sb_{12}$. *J. Appl. Phys.* **99,** 053711-053711-053714 (2006).
24. Chen, L. *et al.* Anomalous barium filling fraction and *n-type* thermoelectric performance of $Ba_yCo_4Sb_{12}$. *J. Appl. Phys.* **90,** 1864–1868 (2001).
25. Li, H., Tang, X., Zhang, Q. & Uher, C. High performance $In_xCe_yCo_4Sb_{12}$ thermoelectric materials with *in situ* forming nanostructured InSb phase. *Appl. Phys. Lett.* **94,** 102114 (2009).
26. Shi, X. *et al.* Low thermal conductivity and high thermoelectric figure of merit in *n-type* $Ba_xYb_yCo_4Sb_{12}$ double-filled skutterudites. *Appl. Phys. Lett.* **92,** 182101 (2008).
27. Dyck, J. S. *et al.* Thermoelectric properties of the *n-type* filled skutterudite $Ba_{0.3}Co_4Sb_{12}$ doped with Ni. *J. Appl. Phys.* **91,** 3698–3705 (2002).
28. Singh, D. J. & Du, M.-H. Properties of alkaline-earth-filled skutterudite antimonides: $A(FeNi)_4Sb_{12}$ (A= Ca, Sr, and Ba). *Phys. Rev. B* **82,** 075115 (2010).
29. Yang, J., Wang, S., Yang, J., Zhang, W. & Chen, L. Electron and Phonon Transport in n-and p-type Skutterudites. in *MRS Proceed.* **1490,** 9–18 ((Cambridge Univ Press,).(2013).
30. Joffe, A. Heat transfer in semiconductors. *Can. J. Phys.* **34,** 1342–1355 (1956).
31. Shanks, H., Maycock, P., Sidles, P. & Danielson, G. Thermal conductivity of silicon from 300 to 1400 K. *Phys. Rev.* **130,** 1743 (1963).
32. Dismukes, J., Ekstrom, L., Steigmeier, E., Kudman, I. & Beers, D. Thermal and Electrical Properties of Heavily Doped Ge-Si Alloys up to 1300 °K. *J. Appl. Phys.* **35,** 2899–2907 (1964).
33. Nikitin, E., Tamarin, P. & Tarasov, V. Thermal and electrical properties of cobalt monosilicide between 4.2 and 1600 K. *Sov. Phys. Solid. Stat.* **11,** 2002–2004 (1970).
34. Martin, J. Thermal conductivity of Mg_2Si, Mg_2Ge and Mg_2Sn. *J. Phys. Chem. Solids* **33,** 1139–1148 (1972).
35. Yelgel, Ö. C. & Srivastava, G. Thermoelectric properties of *n-type* $Bi_2(Te_{0.85}Se_{0.15})_3$ single crystals doped with CuBr and SbI_3. *Phys. Rev. B* **85,** 125207 (2012).
36. Jiang, J., Chen, L., Bai, S., Yao, Q. & Wang, Q. Thermoelectric properties of textured *p-type* $(Bi,Sb)_2Te_3$ fabricated by spark plasma sintering. *Scrip. Mater.* **52,** 347–351 (2005).
37. Wang, S. *et al.* Enhanced thermoelectric properties of $Bi_2(Te_{1-x}Se_x)_3$-based compounds as *n-type* legs for low-temperature power generation. *J. Mater. Chem.* **22,** 20943–20951 (2012).
38. Puneet, P. *et al.* Preferential Scattering by Interfacial Charged Defects for Enhanced Thermoelectric Performance in Few-layered *n-type* Bi_2Te_3. *Sci. Rep.* **3,** 3212; DOI:10.1038/srep03212 (2013).
39. Wang, S. *et al.* Anisotropic multicenter bonding and high thermoelectric performance in electron-poor CdSb. *Chem. Mater.* **27,** 1071–1081 (2015).
40. Kingery, W. D. *Introduction To Ceramics*. (John Wiley & Sons, New York, 1960).
41. Crank, J. *The Mathematics of Diffusion*. (Clarendon Press, Oxford, 1975).
42. Fistul, V. I. *Heavily doped semiconductors*. (Plenum Press, New York, 1969).
43. Ioffe, A. F. *Physics of Semiconductors*. (Academic Press, New York, 1960).
44. Goldsmid, H. J. *Electronic Refrigeration*. (Pion Limited, London, 1986).
45. Goldsmid, H. & Sharp, J. Estimation of the thermal band gap of a semiconductor from Seebeck measurements. *J. Electron. Mater.* **28,** 869–872 (1999).
46. Blakemore, J. S. *Semiconductor Statistics*. (New York, Courier Dover Publications, 2002).
47. Caillat, T., Borshchevsky, A. & Fleurial, J. P. Properties of single crystalline semiconducting $CoSb_3$. *J. Appl. Phys.* **80,** 4442–4449 (1996).
48. Yang, J., Meisner, G., Morelli, D. & Uher, C. Iron valence in skutterudites: Transport and magnetic properties of $Co_{1-x}Fe_xSb_3$. *Phys. Rev. B* **63,** 014410 (2000).
49. Zhou, C., Morelli, D., Zhou, X., Wang, G. & Uher, C. Thermoelectric properties of *P-type* Yb-filled skutterudite $Yb_xFe_yCo_{4-y}Sb_{12}$. *Intermetallics* **19,** 1390–1393 (2011).
50. Yang, K. *et al.* Synthesis and thermoelectric properties of double-filled skutterudites $Ce_yYb_{0.5-y}Fe_{1.5}Co_{2.5}Sb_{12}$. *J. Alloy. Compd.* **467,** 528–532 (2009).
51. Leszczynski, J. *et al.* Electronic band structure, magnetic, transport and thermodynamic properties of In-filled skutterudites $In_xCo_4Sb_{12}$. *J. Phys. D Appl. Phys.* **46,** 495106 (2013).

52. Salvador, J., Yang, J., Wang, H. & Shi, X. Double-filled skutterudites of the type $Yb_xCa_yCo_4Sb_{12}$: Synthesis and properties. *J. Appl. Phys.* **107,** 043705 (2010).
53. Pei, Y. *et al.* Improving thermoelectric performance of caged compounds through light-element filling. *Appl. Phys. Lett.* **95,** 042101 (2009).
54. Pei, Y., Chen, L., Bai, S., Zhao, X. & Li, X. Effect of Pd substitution on thermoelectric properties of $Ba_{0.3}Pd_xCo_{4-x}Sb_{12}$. *Script. Mater.* **56,** 621–624 (2007).
55. Zhao, W. *et al.* Enhanced thermoelectric performance in barium and indium double-filled skutterudite bulk materials via orbital hybridization induced by indium filler. *J. Am. Chem. Soc.* **131,** 3713–3720 (2009).
56. Yang, J. *et al.* Low temperature transport and structural properties of misch-metal-filled skutterudites. *J. Appl. Phys.* **102,** 083702 (2007).
57. Kuznetsov, V., Kuznetsova, L. & Rowe, D. Effect of partial void filling on the transport properties of $Nd_xCo_4Sb_{12}$ skutterudites. *J. Phys. Condens. Mat.* **15,** 5035–5048 (2003).
58. Nolas, G., Cohn, J. & Slack, G. Effect of partial void filling on the lattice thermal conductivity of skutterudites. *Phys. Rev. B* **58,** 164 (1998).
59. Morelli, D. T., Meisner, G. P., Chen, B., Hu, S. & Uher, C. Cerium filling and doping of cobalt triantimonide. *Phys. Rev. B* **56,** 7376 (1997).
60. Slack, G. A. & Hussain, M. A. The maximum possible conversion efficiency of silicon-germanium thermoelectric generators. *J. Appl. Phys.* **70,** 2694–2718 (1991).
61. Xie, W. *et al.* Identifying the specific nanostructures responsible for the high thermoelectric performance of $(Bi,Sb)_2Te_3$ nanocomposites. *Nano Lett.* **10,** 3283–3289 (2010).
62. Snyder, G. J. & Toberer, E. S. Complex thermoelectric materials. *Nat. Mater.* **7,** 105–114 (2008).
63. Dresselhaus, M. S. *et al.* New Directions for Low-Dimensional Thermoelectric Materials. *Adv. Mater.* **19,** 1043–1053 (2007).
64. Yang, J., Yip, H. L. & Jen, A. K. Y. Rational design of advanced thermoelectric materials. *Adv. Energy Mater.* **3,** 549–565 (2013).
65. Minnich, A., Dresselhaus, M., Ren, Z. & Chen, G. Bulk nanostructured thermoelectric materials: current research and future prospects. *Energy Environ. Sci.* **2,** 466–479 (2009).
66. Yang, J. *et al.* Trends in electrical transport of *p-type* skutterudites RFe_4Sb_{12} (R= Na, K, Ca, Sr, Ba, La, Ce, Pr, Yb) from first-principles calculations and Boltzmann transport theory. *Phys. Rev. B* **84,** 235205 (2011).
67. Sofo, J. & Mahan, G. Electronic structure of $CoSb_3$: A narrow-band-gap semiconductor. *Phys. Rev. B* **58,** 15620 (1998).
68. Wang, S., Li, H., Lu, R., Zheng, G. & Tang, X. Metal nanoparticle decorated *n-type* Bi_2Te_3-based materials with enhanced thermoelectric performances. *Nanotechnology* **24,** 285702 (2013).
69. Wang, S., Xie, W., Li, H. & Tang, X. Enhanced performances of melt spun $Bi_2(Te,Se)_3$ for *n-type* thermoelectric legs. *Intermetallics* **19,** 1024–1031 (2011).
70. Wang, S., Xie, W., Li, H. & Tang, X. High performance *n-type* $(Bi,Sb)_2(Te,Se)_3$ for low temperature thermoelectric generator. *J. Phys. D Appl. Phys.* **43,** 335404 (2010).
71. Poudel, B. *et al.* High-thermoelectric performance of nanostructured bismuth antimony telluride bulk alloys. *Science* **320,** 634–638 (2008).
72. Bahk, J.-H. & Shakouri, A. Enhancing the thermoelectric figure of merit through the reduction of bipolar thermal conductivity with heterostructure barriers. *Appl. Phys. Lett.* **105,** 052106 (2014).
73. Zhang, Y., Ke, X., Chen, C., Yang, J. & Kent, P. R. Nanodopant-induced band modulation in $AgPb_mSbTe_{2+m}$-type thermoelectrics. *Phys. Rev. Lett.* **106,** 206601 (2011).
74. Perdew, J. P., Burke, K. & Ernzerhof, M. Generalized gradient approximation made simple. *Phys. Rev. Lett.* **77,** 3865 (1996).
75. Blöchl, P. E. Projector augmented-wave method. *Phys. Rev. B* **50,** 17953 (1994).
76. Kresse, G. & Joubert, D. From ultrasoft pseudopotentials to the projector augmented-wave method. *Phys. Rev. B* **59,** 1758 (1999).
77. Kresse, G. & Furthmüller, J. Efficient iterative schemes for ab initio total-energy calculations using a plane-wave basis set. *Phys. Rev. B* **54,** 11169 (1996).
78. Yang, J. *et al.* Evaluation of Half-Heusler Compounds as Thermoelectric Materials Based on the Calculated Electrical Transport Properties. *Adv. Funct. Mater.* **18,** 2880–2888 (2008).

Acknowledgements

This work was supported by US Department of Energy under corporate agreement DE-FC26-04NT42278, by GM, and by National Science Foundation under award number 1235535.

Author Contributions

Jihui Yang designed research; S.W., Jiong Yang, and T.T. performed research; Jihui Yang, W.Z. and X.T. analyzed data; and Jihui Yang, S.W., and Jiong Yang wrote the paper. All authors reviewed the manuscript.

Additional Information

Supplementary information accompanies this paper at http://www.nature.com/srep

Competing financial interests: The authors declare no competing financial interests.

How to cite this article: Wang, S. *et al.* Conductivity-limiting bipolar thermal conductivity in semiconductors. *Sci. Rep.* **5**, 10136; doi: 10.1038/srep10136 (2015).